# RTM imaging condition using impedance sensitivity kernel combined with Poynting vector

Reynam Pestana*, Adriano W. G. dos Santos, CPGG/UFBA and INCT-GP/CNPQ and Edvaldo S. Araujo, CPGG/UFBA



## Abstract

**Reverse time migration (RTM) using cross-correlation imaging condition is always contaminated by low-spatial-frequency artifacts due to the presence of sharp wave-speed contrasts in the velocity model. Different techniques have been used and Laplacian filtering can lead to good results but it might damage the signal of interest. Recently it has been observed through numerical examples that RTM images obtained using the impedance sensitivity kernel are much less contaminated by low-frequency artifacts. In this work, we are proposing to use the impedance sensitivity kernel instead of the conventional cross-correlation RTM imaging condition to attenuate the low frequency artifacts. Using the impedance sensitivity kernel for the source downgoing wavefield separated by the Poynting vector, we demonstrate through synthetic examples that RTM image results preserve well the reflections and attenuate significantly the backscattered low frequency noise.**

## Introduction

It is well known that reverse time migration (RTM) images suffer from low-spatial-frequency artifacts if two-way wave equations are used. Those artifacts are more prominent with sharp impedance contrasts. Thus, the quality of the resulting image depends on the methodology applied to separate the reflection data from the backscattered low frequency noise produced at each time step by cross-correlating the source and the receivers wavefields.

Baysal et al. (1984) introduced a non-reflecting wave equation with effective results for post-stack migration but not effective for prestack depth RTM, due to the low frequency noise generating mechanism. In recent years, more attention has been given to improve the imaging condition and reduce the low frequency noise. Other techniques have been proposed in literature to eliminate or attenuate these artifacts, for example: a velocity smoothing high-pass filter (Mulder and Plessix, 2004), Poynting vectors (Yoon and Marfurt, 2006), directional damping term at the interface (Fletcher et al., 2006) and high-pass filtering (Guitton et al., 2007).

Another way to address this problem is to modify the imaging condition. In this direction, Liu et al. (2011) proposed an imaging condition based on the decomposition of the wavefield into one-way components correlating only the images related to the reflections. More recently, Whitmore and Crawley (2012) presented a new imaging method based on two images: one is the product of the time derivatives of the source and receivers wavefields and another is the product of the spatial gradients of the source and the receivers wavefields. The images are then combined to produce a final image. This method is called inverse scattering image and it is based on a generalized inverse scattering theory (Stolk et al., 2009).

Lailly (1983) and Tarantola (1984) recognized that the gradient of the least-squares misfit function, or Fréchet derivatives - also referred as sensitivity kernels, used in inversion of seismic reflection waveform data, is closely related to an image in seismic migration based on the imaging principle of Claerbout (1971). Luo et al. (2009) and Zhu et al. (2009) explored this relationship between imaging and inversion and showed numerical examples much less contaminated by low frequency noise using the impedance sensitive kernel. Later on, Douma et al. (2010) showed for an isotropic acoustic medium with constant density that the impedance kernel, away from the source and for a smooth background medium, is identical to the image obtained by applying the Laplacian to a reverse-time migration. Thus, the Laplacian filtering used in practical RTM to attenuate the above-mentioned low-frequency artifacts is very close connected to the impedance sensitivity kernel.

In this paper, we demonstrate by means of numerical examples that the RTM images produced by the imaging condition based on the impedance sensitivity kernel combined with the Poynting vector filtering approach can reduce significantly the low-spatial artifacts mentioned above. We also applied the rapid expansion method (REM) (Pestana and Stoffa, 2010) in order to get a highly accurate solution of the wave equation for the pressure wavefield. In our REM implementation we can also obtain the time derivative of the pressure wavefield required by the new imaging condition with negligible extra computational cost. Using synthetic dataset examples we demonstrate the effectiveness of our imaging implementation to reduce this backscattered correlation noise.

## Reverse time prestack depth migration

By using the full wave equation, RTM implicitly includes multipath arrivals and has no dip limitation, enabling the imaging of complex reflectors. RTM is achieved by a forward and reverse time propagation of source ($P_F$) and

receivers ($P_B$) wavefileds followed by an imaging condition.

To obtain a stable solution of the wave equation even for large time steps, we employ the rapid expansion method (REM) to extrapolate wavefields in time (Pestana and Stoffa, 2010). The spatial derivatives in the wave equation are calculated by the Fourier method and combining it with REM we get a highly accurate solution of the wave equation in a time-stepping manner.

In RTM, the cross-correlation imaging condition, which is given by:

$$I_{cc}(\mathbf{x}) = \int P_F(\mathbf{x},t) P_B(\mathbf{x},t)\, dt \tag{1}$$

is used in practice and is often preferable due to stability reasons. However, RTM imaging condition using correlation method is negatively affected by backscattered and turning waves in the modeling process, which causes the incident and reflected wavefields to be in phase at locations that are not reflection points resulting in strong correlation noise in the seismic image (Whitmore and Crawley, 2012).

### Impedance sensitivity kernel imaging condition and Poynting vector

Based on the relationship of inversion and imaging (Luo et al., 2009; Zhu et al., 2009; Whitmore and Crawley, 2012), we propose the following imaging condition for RTM:

$$\begin{aligned} I_k(\mathbf{x}) &= \frac{1}{v^2(\mathbf{x})} \int \frac{\partial}{\partial t} P_F(\mathbf{x},t)\, \frac{\partial}{\partial t} P_B(\mathbf{x},t)\, dt \\ &+ \int \nabla P_F(\mathbf{x},t).\, \nabla P_B(\mathbf{x},t)\, dt \end{aligned} \tag{2}$$

Equation 2 requires that one calculates not only source and receivers wavefields but also their time derivatives. Using the REM we can obtain the time derivative with negligible extra computational cost (Tessmer, 2011).

Yoon and Marfurt (2006) suggested the use of the Poynting vector to reduce RTM artifacts. Using the direction of propagation of the source and receivers wavefields, we can compute the Poynting vector information to improve the image quality. For the acoustic wave equation, the Poynting vector $\mathbf{S}$ is given by (Yoon and Marfurt, 2006):

$$\mathbf{S} = -\nabla P \frac{\partial P}{\partial t} \tag{3}$$

With the information of propagation direction obtained by the Poynting vector we can separate the source and receivers wavefields into their upgoing and downgoing components and apply the imaging condition for the separated components.

### Numerical results

In this part, we show the RTM results for two synthetic datasets obtained through different imaging conditions procedures. First we show the results for the Marmousi dataset. In Figure 1(a) the result of RTM with artifacts resulting from the cross-correlation imaging condition given by equation 1. The image is contaminated throughout with a very low-frequency noise. In Figure 1(b) we show the RTM result using the Laplacian filtering which shows a good attenuation of the migration artifacts. This filter has two major effects: (1) it increases the high-frequency noise and (2) it removes the low-frequency information (Guitton et al., 2007). To avoid these kind of effects, we have borrowed from inversion the impedance sensitivity kernel and the RTM result using imaging condition with equation 2 is shown in the Figure 3(a). However, the low frequency noise was not completely attenuated. To improve the RTM result we applied the Poynting vector to separate the source and receivers wavefields into their upgoing and downgoing components. The result of the RTM using the impedance kernel applied for the source and receivers downgoing wavefields can be seen in the Figure 1(d). The noise was attenuated, but again not completely and it also damaged some reflections. The receiver Poynting vector is difficult to be accurately computed, because the receivers wavefield tend to point in many different directions at one time and location. Using only the separated downgoing source wavefield with the impedance kernel we obtained a much cleaner result (Figure 1(e)).

To show the major effects of the Laplacian filter, we also applied the same imaging condition described above to the Sigsbee2a dataset. Figure 2(a) is the conventional imaging condition result and the noise is particularly strong where the salt body is presented. Figure 3(a) shows its 2D spectrum. The Laplacian filtering result is shown in Figure 2(b) and its FK plot (Figure 3(b)) shows the strong attenuation of the low-frequency components at $k_z = 0$ and $k_x = 0$. Figures 2(c) and 2(d) show the results for the impedance kernel (equation 2) using the complete source wavefield and the source separated downgoing wavefield, respectively. Comparing the FK plots of the RTM results with the Laplacian filtering (Figure 3(b)) and the RTM result with impedance kernel with the source separated downgoing wavefield (Figure 3(c)), we can see in Figure 3(c) that the spectrum of the RTM result is well preserved and has less attenuation at $k_z = 0$ and $k_x = 0$.

### Conclusions

Reverse time migration produces low-frequency artifact using the conventional cross-correlation imaging condition. The practical Laplacian filter is easy to apply and can remove these artifacts but it can damage the signal of interest. In this work, we proposed to use the impedance sensitivity kernel to replace the conventional cross-correlation and attenuate the low frequency artifacts. We demonstrated with synthetic examples that the RTM results obtained with impedance kernel for the downgoing wavefield separated using the Poynting vector can preserve the reflections and attenuate the low frequency artifacts. The proposed imaging condition can be cheaply applied during the migration procedure.

### Acknowledgements

This research was supported by CNPq and INCT-GP/CNPq. The facility support from CPGG/UFBA is also acknowledged.

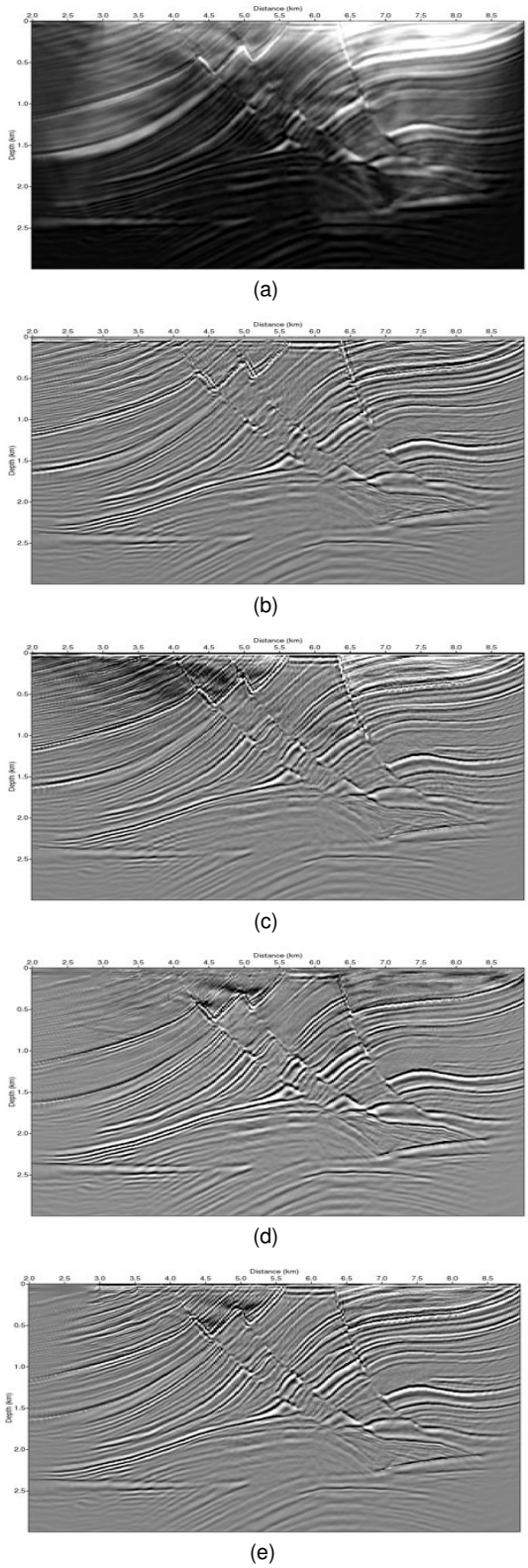


(a) (b) (c) (d) (e)

Figure 1: Marmousi RTM result using: (a) Conventional imaging condition (cross-correlation); (b) Conventional imaging condition plus Laplacian filter; (c) Imaging condition based on the impedance sensitivity kernel; (d) Impedance sensitivity kernel applied for source and receivers separated downgoing wavefields and (e) Impedance sensitive kernel applied only for the source separated downgoing wavefield.

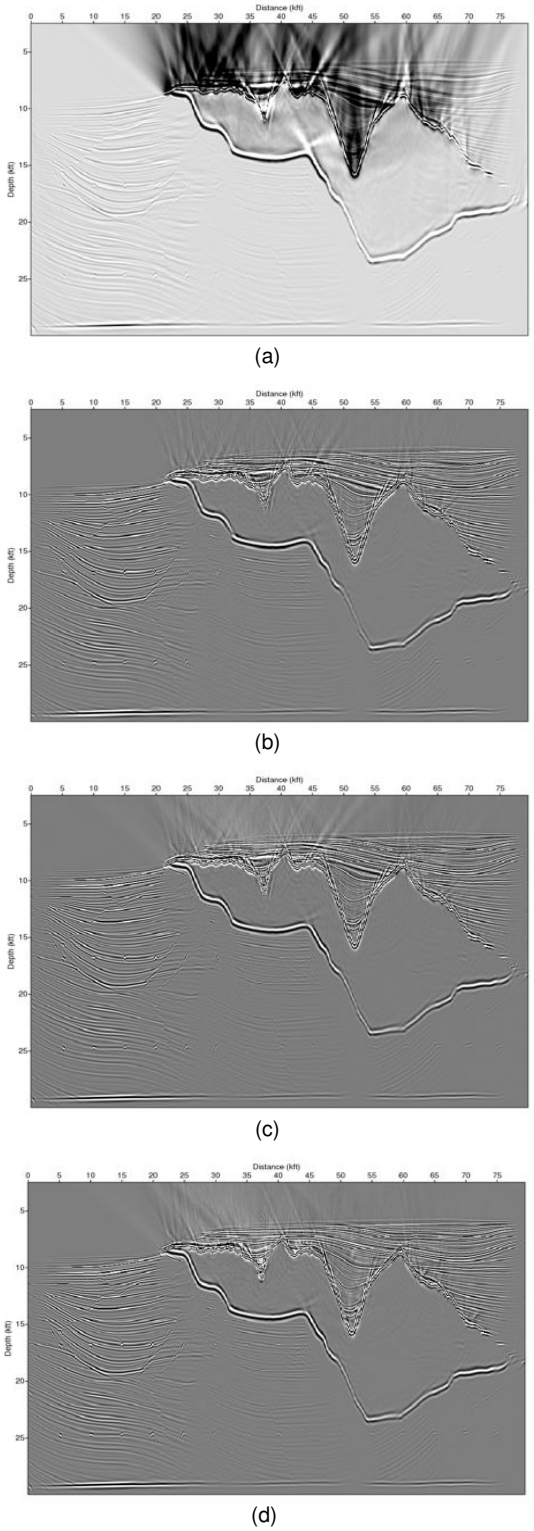


(a) (b) (c) (d)

Figure 2: Sigsbee2a RTM result with: (a) Conventional imaging condition (cross-correlation); (b) Conventional imaging condition plus Laplacian filter; (c) Imaging condition based on the impedance sensitivity kernel; (d) Impedance sensitivity kernel imaging using only the source separated downgoing wavefield.

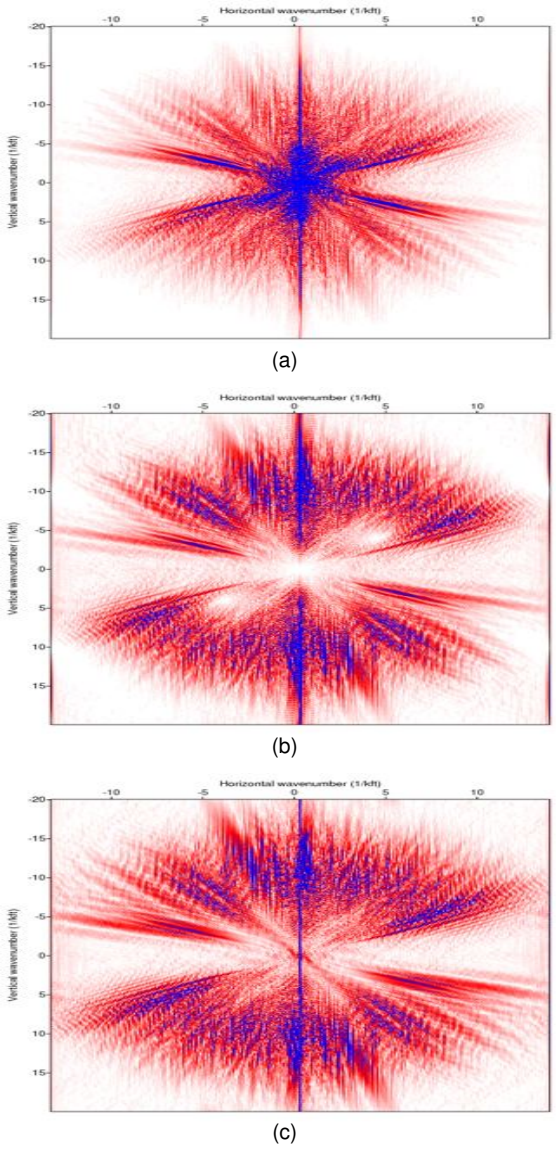


Figure 3: 2-D Fourier spectrum of Sigsbee2a dataset after: (a) Conventional imaging condition; (b) Conventional imaging condition plus Laplacian filter and (c) Impedance sensitivity kernel imaging using only the source separated downgoing wavefield.

## References


Baysal, E., D. D. Kosloff, and J. W. C. Sherwood, 1984, A two-way nonreflecting wave equation: Geophysics, **49**, 132–141.

Claerbout, J., 1971, Toward a unified theory of reflector mapping: Geophysics, **36**, 467–481.

Douma, H., D. Yingst, I. Vasconcelos, and J. Tromp, 2010, On the connection between artifact filtering in reverse-time migration and adjoint tomography: Geophysics, **75**, S219–S223.

Fletcher, R., P. Fowler, P. Kitchenside, and U. Albertin, 2006, Suppressing unwanted internal reflections in prestack reverse-time migration: Geophysics, **71**, E79–E82.

Guitton, A., B. Kaelin, and B. Biondi, 2007, Least-squares attenuation of reverse-time migration artifacts: Geophysics, **72**, S19–S23.

Lailly, P., 1983, The seismic inverse problem as a sequence of before stack migration: Conference on inverse scattering. Theory and applications: Society for Industrial and Applied Mathematics, **36**, Proceeding, 467–481.

Liu, F., G. Zhang, S. A. Morton, and J. P. Leveille, 2011, An effective imaging condition for reverse-time migration using wavefield decomposition: Geophysics, **76**, S29–S39.

Luo, Y., H. Zhu, , T. Nissen-Meyer, C. Morency, and J. Tromp, 2009, Seismic modeling and imaging based upon spectral-element and adjoint methods: Leading Edge, 568–574.

Mulder, W. A. and R. Plessix, 2004, A comparison between one-way and two-way wave equation migration: Geophysics, **69**, 1491–1501.

Pestana, R. and P. Stoffa, 2010, Time evolution of the wave equation usind rapid expansion method: Geophysics, **75**, T121–T131.

Stolk, C. C., M. V. de Hoop, and Op't Root, 2009, Linearized inverse scattering based on seismic reverse-time migration: Proceeding of the Project Review, Geo-Mathematical Imaging Group - Purdue University.

Tarantola, A., 1984, Inversion of seismic reflection data in the acoustic approximation: Geophysics, **49**, 1259–1266.

Tessmer, E., 2011, Using the rapid expansion method for accurate time-stepping in modeling and reverse-time migration: Geophysics, **76**, S177–S185.

Whitmore, N. D. and S. Crawley, 2012, Application of RTM inverse scattering imaging conditions: 82nd Annual International Meeting, SEG, Expanded Abstracts.

Yoon, K. and K. J. Marfurt, 2006, Reverse-time migration using the poynting vector: Exploration Geophysics, **37**, 102–107.

Zhu, H., Y. Luo, T. Nissen-Meyer, C. Morency, and J. Tromp, 2009, Elastic imaging and time-lapse migration based on adjoint methods: Geophysics, WCA167–WCA177.